The Cl + H_2 → HCl + H Reaction Induced by IR + UV Irradiation of Cl_2 in Solid *para*-H_2: Experiment†

Sharon C. Kettwich,[#,§] Paul L. Raston,[#,‡] and David T. Anderson*[,#,§]

Department of Chemistry, University of Wyoming, Laramie, Wyoming 82071, and Institut für Experimentalphysik, Freie Universität Berlin, Fachbereich Physik, Arnimallee 14, D-14195, Berlin, Germany

Received: December 18, 2008; Revised Manuscript Received: February 23, 2009

We report IR + UV coirradiation photolysis experiments conducted on Cl_2-doped *para*-hydrogen (*p*-H_2) crystals at 1.8 K, using pulsed 355 nm UV radiation and cw broad-band near-IR light from a FTIR tungsten source. The amount of HCl photoproduct is monitored using FTIR spectroscopy as a function of the IR + UV exposure time. Detailed analysis of the HCl growth kinetics reveals that the reaction Cl + H_2(v=1,J=0) → HCl + H is playing a significant (15%) role in the in situ photochemistry. In contrast, UV-only photolysis experiments conducted under similar conditions produce almost exclusively (99%) isolated Cl atom photofragments, indicating the reaction Cl + H_2(v=0,J=0) → HCl + H is not readily occurring. This combination of photolysis experiments confirms that under these conditions, the Cl + H_2 reaction probability increases by a factor greater than 25 for Cl atom reactions with H_2(v=1) versus H_2(v=0). These results are therefore consistent with the expectation that vibrational excitation of the H_2 reagent lowers the reaction threshold and increases the reaction cross section for the Cl + H_2 reaction. These experimental studies were motivated by and are compared to the quantum model simulations reported by Korolkov, Manz, and Schild in the accompanying paper.

1. Introduction

The UV photodissociation of guest molecules in low-temperature rare gas (Rg) matrixes have long served as model systems to probe the microscopic details of condensed-phase photoreaction dynamics.[1,2] The cold and well-ordered Rg crystalline environment permits both precise experiment and theory to be performed on the same molecular system, and the synergy between theory and experiment permits greater insight into the molecular dynamics. Professor R. Benny Gerber has made seminal contributions to the development of theoretical methods used to investigate the photochemistry of small molecules in Rg matrixes for more than 20 years. Gerber and co-workers began with classical molecular dynamics simulations[3,4] using gas-phase pairwise additive potentials, and current theoretical research focuses on nonadiabatic simulation methods that can treat multiple electronic states and many atoms.[5,6] In many ways, *para*-hydrogen (*p*-H_2) crystals, with each H_2 molecule populating a spherical $J = 0$ rotational wave function within the solid, mimic Rg matrixes as simple hosts for photochemical studies with two important differences; (1) the zero-point energy in *p*-H_2 crystals is a significant fraction of the binding energy of the solid, making them quantum crystals,[7] and (2) each *p*-H_2 molecule has an embedded vibrational coordinate that can be excited via IR absorptions of the solid.[8] The experimental work reported here was motivated by theoretical investigations in the group of J. Manz which predicted very different outcomes for Cl_2 photodissociation in *p*-H_2 crystals using UV and IR + UV irradiation schemes.[9]

The Cl + H_2 → HCl + H reaction is a prototypical hydrogen abstraction reaction that has been studied at increasing levels of detail both experimentally and theoretically for more than 100 years.[10,11] The barrier to the Cl + H_2 reaction, corrected for zero-point energy, is ∼1900 cm^{-1}, and the reaction is nearly thermoneutral; it is only +360 cm^{-1} endothermic.[12,13] Recently, this reaction has been the focus of extensive research due to gas-phase experimental studies that indicated significant electron−nuclear coupling in the chemical reaction dynamics.[14,15] However, the most recent report on this reaction shows that nonadiabatic effects are not important and that fully quantum-reactive scattering calculations based on sophisticated reactive potential energy surfaces which include the open-shell character of the Cl(^{2}P) reagent are in excellent agreement with differential reactive scattering cross section measurements.[16] Despite all of the interest in this reaction, the influence of vibrational excitation of the H_2 reagent on the reaction rate and dynamics have not been studied in detail, and the only theoretical predictions of reagent vibrational excitation are based on quasiclassical trajectory studies by Persky, Rubin, and Broida on an early semiempirical potential energy surface.[17] These trajectory studies predict that at 250 K, the rate constant for H_2(v=1) compared to that for H_2(v=0) should increase by a factor of 1120 and that the reaction threshold should drop from ∼1400 cm^{-1} for H_2(v=0) to 350 cm^{-1} for H_2(v=1). The increase in the rate constant for H_2(v=1) is consistent with the Polanyi rules for late barrier reactions, where very significant enhancements in reaction rates are caused by vibrational excitation of the reactants.[18]

Our group has recently been studying the in situ UV photodissociation of Cl_2 in solid *p*-H_2 as a way to prepare isolated Cl atoms in solid *p*-H_2.[19−21] Describing this work while on sabbatical at the Freie Universität in Berlin in 2007−2008, a number of conversations with the Manz group led to the following theoretical prediction. The Manz group predicted that in situ UV photodissociation of Cl_2 in a *p*-H_2 matrix consisting

† Part of the "Robert Benny Gerber Festschrift".

* To whom correspondence should be addressed. E-mail: danderso@uwyo.edu.
[#] University of Wyoming.
[§] Freie Universität Berlin.
[‡] Present address: Department of Chemistry, University of Alberta, Edmonton, Alberta T6G 2G2, Canada.

10.1021/jp811206a CCC: $40.75 © 2009 American Chemical Society
Published on Web 04/20/2009

of $H_2(v=0,J=0)$ molecules should result in the production of isolated Cl atoms. Indeed, this had already been experimentally verified in our group by complete 355 nm photodissociation of 50 ppm Cl_2-doped p-H_2 samples, where the product Cl atoms can be detected by the Cl spin−orbit transition.[19−21] However, the Manz group further predicted that if we carried out UV photodissociation while exposing the solid to IR radiation, the Cl + H_2 reaction rate would become significantly enhanced due to the simultaneous production of translationally hot Cl atoms and vibrationally excited $H_2(v=1)$ molecules.[9] To better understand the significance of these predictions, we should first explore the details of 355 nm photodissociation of Cl_2 in solid p-H_2.

It is known from extensive gas-phase measurements that photodissociation of Cl_2 at 355 nm accesses the C $^1\Pi_{1u}$ repulsive potential energy surface, which correlates with two ground spin−orbit state $Cl(^2P_{3/2})$ atoms.[22−24] Sensitive REMPI measurements of the Cl atom fine-structure branching ratio at this photodissociation wavelength confirm that only 0.6% of the Cl atoms are produced in the excited spin−orbit state $Cl(^2P_{1/2})$.[23] On the basis of these gas-phase measurements, 355 nm photodissociation of Cl_2 in solid p-H_2 using nanosecond pulses from a Nd:YAG laser should produce two $Cl(^2P_{3/2})$ atoms with laboratory frame translation energies of 4090 cm^{-1} given by the conservation of energy

$$E_{trans} = \frac{m(Cl)}{m(Cl_2)}[E_{ph} - D_0] \quad (1)$$

where E_{trans} is the translational energy of the photoejected Cl atom, E_{ph} is the photon energy (3.493 eV), and $D_0 = 2.4793$ eV is the dissociation energy[25] of Cl_2 ($X^1\Sigma_g$). After photodissociation, there are a number of possible further reaction steps as outlined below

$$Cl_2 + h\nu \rightarrow 2Cl^* \quad (2)$$

$$Cl^* + H_2(v = 0, J = 0) \rightarrow HCl + H \quad (3)$$

$$Cl^* + H_2(v = 1, J = 0) \rightarrow HCl + H \quad (4)$$

$$Cl + H_2(v = 1, J = 0) \rightarrow HCl + H \quad (5)$$

The nascent Cl atom is designated Cl* since it is produced at high translational energies within the crystal. The nascent photoejected Cl* atom can react with the p-H_2 matrix via reaction 3 since it is produced with enough translational energy to overcome the barrier to the Cl + H_2 reaction. However, if the photoejected Cl atom does not react and becomes equilibrated in the matrix, it can no longer react with $H_2(v=0,J=0)$ because the Cl + H_2 reaction is endothermic and thus cannot occur at liquid helium temperatures ($kT \approx 2.78$ cm^{-1}) even by a tunneling mechanism.[20] The equilibrated Cl atom can react with $H_2(v=1)$ via reaction 5 since the H_2 vibrational energy can be used to overcome the reaction endothermicity.[19−21] Other reaction schemes leading to the production of HCl aside from those listed above are possible as well. For example, secondary reactions involving the H-atom product with unreacted Cl atoms in the solid are possible, but by keeping the initial Cl_2 concentration low, the rates of these secondary reactions should be slow enough that they can be neglected.

Our group has studied the kinetics of reaction 5 by producing small amounts of $H_2(v=1)$ via irradiation of Cl-atom-doped solid p-H_2 with near-IR light from 4000 to 5000 cm^{-1} using the IR source of a FTIR spectrometer.[19,20] These photochemical studies are unique in that they utilize IR light to vibrationally excite the p-H_2 host to induce reaction 5. Recently, the Räsänen group has also used IR host excitation in solid hydrogen matrixes to promote conformational change in formic acid dopant species.[26] Previous UV photochemical studies in p-H_2 matrixes have been carried out by Fajardo and co-workers, who investigated the formation of water clusters after 193 nm photolysis of O_2-doped p-H_2 crystals.[27] Other studies include those performed by Momose et al., which utilize UV photochemistry to produce methyl radicals in p-H_2 crystals[28−32] in order to explore tunneling reactions of CH_3 with the p-H_2 host. Momose also studied the formation of CO and H_2O from UV photolysis of $HI\cdots CO_2$ complexes[33] in solid p-H_2. However, we are the first to test if vibrational excitation of the matrix host can be used to control the outcome of a chemical reaction in a quantum solid. Specifically, we wanted to see if we could make the Cl + H_2 → HCl + H reaction occur by vibrationally exciting the H_2 reactant.

The question that stimulated the present work was could a simultaneous IR + UV irradiation scheme, using the available cw IR source and pulsed UV laser, be used to "turn on" reaction 4 to the extent that its effect on the HCl photoproduction rate could be measured. This demands that a sufficient population of $H_2(v=1)$ be produced with the IR source so that the nascent Cl* atoms have a finite probability of colliding with a $H_2(v=1)$ molecule before returning to equilibrium within the matrix. Quantifying the minimum concentration of $H_2(v=1)$ necessary to measure an effect depends largely on the degree of reaction enhancement with H_2 vibrational excitation under these conditions. We knew that UV-only photodissociation produced very little HCl via consecutive reactions 2 and 3, so that even a modest vibrational enhancement in the Cl + H_2 reaction might lead to detectable differences in the HCl photoproduction kinetics using an IR + UV coirradiation scheme. We were, however, pessimistic that the weak IR source could produce sufficient amounts of $H_2(v=1)$ to measure an effect.

The cw IR source is quite weak, and the power (∼10 mW) is distributed over a large wavenumber range, but the peak in the intensity distribution is in the near-IR region where solid p-H_2 absorbs (4200−4800 cm^{-1}) creating $H_2(v=1)$. The intermolecular forces between neighboring H_2 molecules within the solid lead to vibrational coupling, and thus, IR absorption by the solid does not result in excitation of singly localized $H_2(v=1)$ molecules, but rather, the excitation is distributed over multiple H_2 molecules simultaneously, and the excitation is delocalized throughout the solid.[8] The stronger the vibrational coupling, the more the $H_2(v=1)$ vibrational amplitude is distributed over greater numbers of H_2 molecules. In p-H_2, the $H_2(v=1)$ vibrational state is broadened into a vibrational exciton band which extends over approximately 4 cm^{-1}, and the exciton is termed a vibron.[8,34,35] Thus, the reaction cross section for a translationally hot Cl* atom with a $v=1$ vibron in solid p-H_2 is likely greater than what it would be if the vibrational excitation was localized on a single $H_2(v=1)$ molecule. The results reported herein have two important ramifications; (1) differences in the outcomes of the UV and IR + UV photolysis experiments indicate that sufficient amounts of $v = 1$ vibrons are generated with the IR source to alter the photochemistry, and (2) these differences occur because IR + UV coirradiation results in some of the photoejected Cl* atoms reacting with $v = 1$ vibrons

while the Cl* atoms are still translationally hot. Again, we would like to emphasize that we would not have conducted these experiments if it were not for the predictions of the Manz group.[9]

2. Experimental Section

The methods[36,37] used to prepare Cl_2-doped p-H_2 crystals have been reported previously,[20,38] and here, we will focus on the specifics of the IR + UV photochemical measurements. In brief, the crystals are synthesized by codepositing independent gas flows of Cl_2 and precooled p-H_2 (99.99%) gas onto a BaF_2 substrate maintained at ~2.5 K with a sample-in-vacuum liquid helium bath cryostat. The gas flow rates are adjusted to grow approximately 2.5(1) mm thick samples with Cl_2 concentrations of ≤50 ppm. The concentration of Cl_2 was kept below 50 ppm to work within the dilute matrix isolation limit in order to minimize Cl atom recombination during UV photolysis and to minimize the importance of secondary reactions involving the H-atom products. The samples were not thermally annealed and thus exhibit a crystal morphology consisting of mixed hexagonal close-packed and face-centered cubic structures.[39]

In order to study the IR + UV-induced HCl photoproduction kinetics, two different types of experiments were performed. The first experiment, designated UV, involved UV photolysis of the sample in the absence of any external IR light source in order to examine the kinetics of reactions 2 and 3. UV photolysis is achieved using the 355 nm output of a 10 Hz Nd:YAG laser (Spectra Physics Laboratory-170-10) with approximately 7−8 ns pulse widths. The unfocused 8 mm diameter UV laser beam is adjusted to an energy of 4(±0.5) mJ per pulse as measured with a power meter just before a CaF_2 photolysis window on the vacuum shroud of the helium cryostat. The UV beam impinges on the crystal at 45° with respect to the surface normal of the BaF_2 substrate. In the UV photolysis experiments, the sample is irradiated in 5 min exposure intervals while maintaining the sample at 1.8 K. After each UV photolysis exposure, the amount of HCl produced is measured using a FTIR spectrometer (Bruker IFS 120 HR) with appropriate filters in the IR beam to prevent HCl production via reaction 5.[19−21] This procedure is repeated for up to 1 h total of UV exposure to fully photodissociate all of the Cl_2 molecules in the sample. After the UV photolysis is complete, the sample is exposed to unfiltered IR light from the FTIR spectrometer to chemically transform all of the unreacted Cl atoms into HCl so that the maximum HCl infrared absorption signal can be measured. This allows the HCl signal produced from UV photolysis to be compared to the total HCl signal that would be produced if all of the Cl atoms were to react to form HCl. The latter process is designated IR, and the IR-induced reaction 5 is achieved with the unfiltered cw IR output from the FTIR spectrometer equipped with a CaF_2 beamsplitter and tungsten source with a 4.0 mm aperture setting on the IR source. This combination of beamsplitter and IR source produces broad-band near-IR radiation with peak intensity in the 4000−5000 cm^{-1} range where solid p-H_2 absorbs. The IR beam is focused with 90° off-axis parabolic mirrors to a nominal spot size of around 1−2 mm diameter within the UV-irradiated part of the crystal. The sample is IR irradiated for time periods ranging from 1 to 60 min for a total IR exposure time of up to 4 h. This experiment allows us to study the UV- and IR-induced HCl production kinetics separately.

The second type of experiment performed is designated IR + UV and consists of simultaneous exposure of the Cl_2-doped p-H_2 sample to both the IR and UV sources for specific time intervals ranging from 5 s to 1 h, for up to ~3 h of total IR + UV exposure. Once again, the sample is maintained at 1.8 K, and after each IR + UV exposure, the amount of HCl produced is measured using the FTIR with appropriate filters in the IR beam. The energy of the UV laser is adjusted to 4(±0.5) mJ per pulse to match the conditions of the UV photolysis experiments, and the IR light is generated using the FTIR with a CaF_2 beamsplitter and unfiltered tungsten source with a 12.5 mm aperture setting. The IR + UV experiments allow for the investigation of the amount of HCl produced by consecutive reactions 2 and 4.

The HCl concentration is monitored during both UV and IR + UV experiments using the FTIR spectrometer equipped with a tungsten source, a CaF_2 beamsplitter, and a liquid-nitrogen-cooled InSb detector. Raston has shown previously that with a 3861 cm^{-1} long-pass filter (LPF) in the IR beam, there is practically no IR light at frequencies greater than 4000 cm^{-1} impinging on the crystal, so that under these conditions, reaction 5 is not induced at a measurable rate.[20] Thus, by filtering the tungsten source with the 3861 cm^{-1} LPF, we are able to nonintrusively monitor the HCl concentration within the sample using the $R_1(0)$ transition at around 2894 cm^{-1} without complications arising from the IR-induced reaction of Cl atoms present in the sample.[40] All spectra, therefore, are recorded from 1900 to 3900 cm^{-1} with a 3861 cm^{-1} LPF in the IR beam and are averaged over 36 scans with 0.05 cm^{-1} resolution. The IR beam is propagated through the BaF_2 deposition substrate and sample with the main optical axis parallel to the substrate surface normal (0° incidence). The entire optical path outside of the FTIR and cryostat vacuum shroud is purged with dry N_2 gas to reduce atmospheric absorptions.

3. Results

(a) UV Photolysis. The extent of the $Cl + H_2$ reaction under either UV or IR + UV photolysis conditions will be monitored by measuring the integrated absorption of the $R_1(0)$ rovibrational transition of HCl. The infrared spectrum of HCl isolated in solid p-H_2 has been measured previously, and HCl was found to undergo nearly free rotation.[40] At liquid helium temperatures, only the $J = 0$ ground rotational state is populated, so that the total HCl concentration can be monitored using the single $R_1(0)$ transition. The $R_1(0)$ absorptions for $H^{37}Cl$ and $H^{35}Cl$ occur at 2892.06 and 2894.19 cm^{-1}, respectively.[40] Infrared spectra of a 42 ppm Cl_2-doped p-H_2 solid in the HCl region (2820−2920 cm^{-1}) are shown in Figure 1 at various steps throughout a UV photolysis experiment. Trace (a) in Figure 1 is for the as-deposited Cl_2-doped p-H_2 sample recorded at 1.83 K and demonstrates that negligible amounts of HCl are produced during Cl_2/p-H_2 deposition. The spectrum in trace (b) of Figure 1 is recorded after 41 min of UV photolysis at 1.83 K and shows that only a small amount of HCl is produced. Note that the absorption intensity in both traces (a) and (b) of Figure 1 has been multiplied by a factor of 5 to more easily demonstrate the modest increase in the HCl $R_1(0)$ signal upon UV photolysis. In addition, UV photolysis produces a number of sharp features near 2836 cm^{-1} which can be assigned to the HCl donor mode of $(HCl)_2$.[40] However, in trace (b) of Figure 1, the integrated absorbance of these sharp dimer peaks is only 25% of the HCl $R_1(0)$ monomer line. Given that the absorption strength of this dimer feature is likely 2.5 times stronger than the monomer line,[41] this indicates that the majority (90%) of the UV-photoproduced HCl is well-isolated and the integrated absorption of the $R_1(0)$ transition is an accurate measure of the relative HCl concentration.

The next step is to determine the amount of HCl that would have been produced if all of the photoejected Cl atoms had

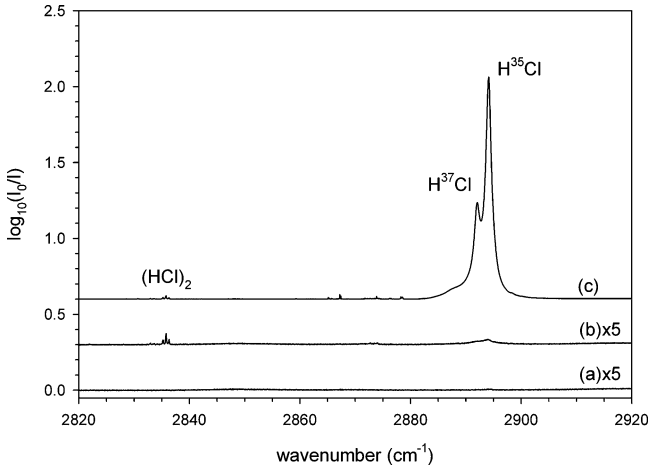

Figure 1. IR spectra in the HCl region for a 42 ppm Cl_2-doped p-H_2 solid recorded at 1.83 K at various steps throughout a UV photolysis experiment. (a) As-deposited sample before UV photolysis. (b) After 41 min of 10 Hz UV photolysis at 4.0 mJ pulse^{-1}. The absorption intensities in traces (a) and (b) have been multiplied by a factor of 5 to show the HCl $R_1(0)$ absorption. (c) The same sample after 221 min of IR irradiation with the unfiltered tungsten source.

reacted with H_2 to form HCl. We estimate that it should take roughly 11.3 min to photodissociate 99% of the Cl_2 dopant under these conditions based on the Cl_2 absorption cross section at 355 nm (16.2×10^{-20} cm^2 molecule^{-1}),[42] the UV laser flux (1.4×10^{17} photons cm^{-2} s^{-1}) for a 4 mJ per pulse 10 Hz 355 nm laser beam with a 4 mm radius, and the measured Cl-atom photoproduction quantum yield ($\Phi = 0.3$) for Cl_2 in solid p-H_2.[43] Since the UV photolysis is conducted for a total of 41 min, we assume that all of the Cl_2 molecules have photodissociated. After UV photolysis is complete, the UV laser is turned off, and unfiltered IR light from the FTIR spectrometer is irradiated onto the sample for specified time intervals to cause the equilibrated Cl atoms to react with vibrationally excited $H_2(v=1)$ via reaction 5 to form HCl. Trace (c) in Figure 1 illustrates that the integrated absorbance of the HCl $R_1(0)$ absorption for the UV-photolyzed sample becomes significantly greater after 221 min of IR exposure. The $(HCl)_2$ peaks around 2836 cm^{-1} only increase by a factor of 1.8 upon IR irradiation, suggesting that reaction 5 does not induce significant diffusion or agglomeration of the HCl product molecules. The IR irradiation results confirm that the nascent Cl* atoms produced by in situ UV photolysis only slightly react with the p-H_2 matrix host even though they are produced with a translational energy of 4090 cm^{-1} that far exceeds the barrier to reaction.[20] This lack of reactivity must be a result of the small reaction 3 cross section under these conditions and the high thermal conductivity of solid p-H_2, which very effectively dissipates the excess translational energy imparted to the Cl atoms via photodissociation.[29,44] These results agree with early published results from this group on the in situ UV photodissociation of Cl_2 in p-H_2.[19−21]

To calculate the fraction of HCl produced during UV photolysis via reaction 3, the individual HCl kinetic data for the UV and IR irradiation steps were analyzed separately. The HCl photoproduction rate can be determined by integrating the HCl $R_1(0)$ absorption feature (for both $H^{37}Cl$ and $H^{35}Cl$ isotopomers) from 2880 to 2910 cm^{-1} for spectra recorded at various irradiation times. For both the UV and IR irradiation procedures described above, the HCl production rate is found to be first-order. The experimental data for HCl production are plotted in Figure 2 as open circles and squares for the separate UV and IR irradiation procedures, respectively. An enlargement of the UV photolysis data is shown as an inset in Figure 2. The UV experimental data points are fit to a simple first-order exponential growth expression[45]

$$y = y_0 + a(1 - e^{-kt}) \quad (6)$$

where y_0 denotes the $R_1(0)$ integrated absorbance at time $t = 0$, a is the maximum integrated absorbance at $t = \infty$, and k is the rate constant for HCl production. The solid lines in Figure 2 are the fitted exponential curves from separate least-squares fits of the UV and IR data to eq 6. Note that in fitting the IR data to eq 6, the 41 min UV photolysis time is subtracted from the time for the IR data shown in Figure 2. The fitted parameters are reported in Table 1. Consistent with the assumption that all of the Cl_2 is photodissociated during UV photolysis, the HCl growth curve levels off at around 20 min (see inset in Figure 2) within a factor of 2 of the estimated 11.3 min as stated above. Since the UV photolysis is complete before the IR irradiation is started, the growth curve labeled IR in Figure 2 reflects the growth of HCl due solely to reaction 5. The rate constant extracted from the IR data agrees with previous published results for the IR-induced reaction of Cl atoms trapped in solid p-H_2.[20] The rate constant is measured here to be $k_5 = 0.0134(2)$ min^{-1}, which is only slightly larger than the rate constant (0.00861(5) min^{-1}) reported for IR irradiation of Cl-atom-doped solid p-H_2 using a globar source with a 5500 cm^{-1} LPF in the IR beam at an aperture diameter of 4.0 mm.[20] The slightly larger rate constant measured here likely reflects more IR intensity in the critical 4000−5000 cm^{-1} region, which can be achieved here with the unfiltered light from a tungsten source at an identical aperture setting.

The fitted rate constant for the UV data is an effective rate constant for production of HCl via consecutive reactions 2 and

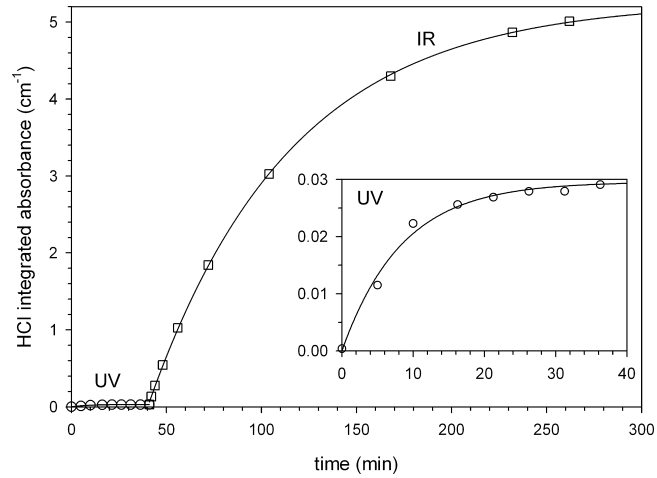

Figure 2. The integrated absorbance of the HCl $R_1(0)$ peak as a function of exposure to first UV light (circles) followed by exposure to IR light (squares) for the same sample depicted in Figure 1. The inset shows an expanded view of the UV photolysis data. The solid lines in Figure 2 are the results of least-squares fits of the data to eq 6. Note that UV photolysis is performed first and separate from the IR irradiation process.

TABLE 1: UV Photolysis Fitted Constants

	y_0/cm^{-1}	a/cm^{-1}	k/min^{-1}
UV	0[a]	0.0296(6)	0.119(10)
IR	0.064(1)	5.21(2)	0.0134(2)

[a] Constrained to 0 in the fit.

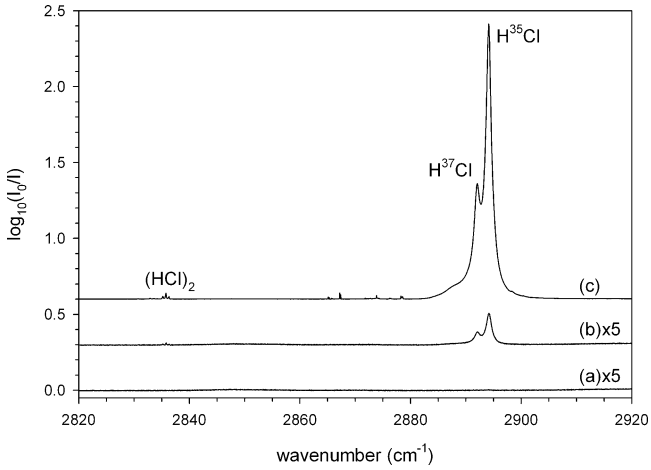

Figure 3. IR spectra in the HCl region for a 42 ppm Cl_2-doped p-H_2 solid recorded at 1.83 K at various steps throughout an IR + UV photolysis experiment. (a) As-deposited sample before IR + UV coirradiation. (b) After 20 s of IR + UV irradiation. Traces (a) and (b) have been multiplied by a factor of 5 for magnification of HCl features. (c) Sample after 164 min of IR + UV irradiation.

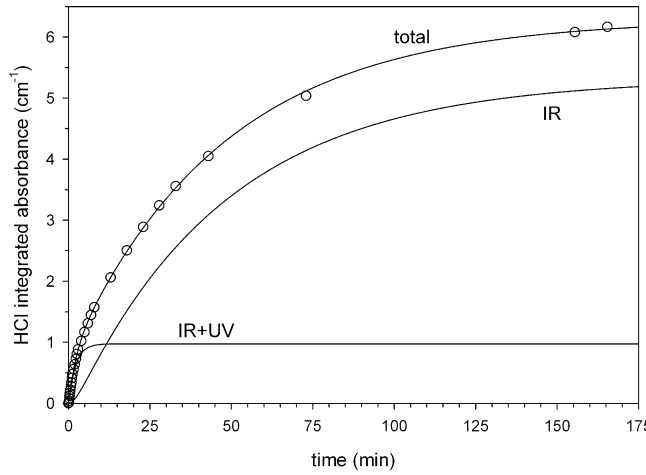

Figure 4. The integrated absorbance of the HCl $R_1(0)$ peak as a function of exposure to IR + UV coirradiation for the same sample depicted in Figure 3. Here, the sample was exposed to both IR and UV light simultaneously. The experimental data points are plotted as open circles, and the solid lines are the result of fits of the data to eq 8. See text for details.

3. The individual rate constants cannot be extracted from the data, and thus instead, the reaction probability for reaction 3 can be estimated from the amount of HCl produced during the UV and IR steps in the photolysis procedure illustrated in Figure 2. For this calculation, we will use the fitted parameters to estimate the amount of HCl produced during the two-step photolysis experiment. The fraction of HCl produced via reaction 3 during UV photolysis can be calculated using the parameters reported in Table 1 and the following expression

$$P_R^{UV} = \frac{a^{UV}}{(y_0^{IR} + a^{IR})} \quad (7)$$

where a^{UV} is the maximum $R_1(0)$ integrated absorbance for UV photolysis and $(y_0^{IR} + a^{IR})$ is the maximum integrated absorbance after sequential UV and IR irradiation. For the data shown in Figure 2, the value is found to be $P_R^{UV} = 0.0056(1)$. This analysis procedure is self-normalizing and thus accounts for small differences in the initial Cl_2 concentration and crystal thickness in order to compare experiments conducted on different crystals. In addition to the data presented in Figure 2 and Table 1, we analyzed four other UV photolysis experiments with approximately 50 ppm initial Cl_2 concentrations and found $P_R^{UV} = 0.0061(30)$, where the uncertainty in parentheses represents the 2σ value for the five separate experiments. This demonstrates that very little HCl is produced during UV photolysis of Cl_2 in solid p-H_2 at 1.8 K if care is taken to make sure that the sample is not exposed to IR radiation in the 4000−5000 cm^{-1} range during the UV photolysis step.

(b) IR + UV Photolysis. Next, IR + UV experiments were conducted in order to determine the amount of HCl produced via reaction 4. Analogous to Figure 1, IR spectra of a 42 ppm Cl_2-doped p-H_2 solid in the HCl region are shown in Figure 3 at various steps throughout the IR + UV irradiation procedure. The spectrum in trace (a) of Figure 3 is of the as-deposited Cl_2-doped p-H_2 sample and shows no evidence for any HCl $R_1(0)$ absorption intensity prior to IR + UV irradiation. Similar to Figure 1, the spectra in traces (a) and (b) of Figure 3 have been rescaled by a multiplicative factor of 5. The spectrum in trace (b) of Figure 3 shows the increase in the HCl $R_1(0)$ absorption intensity after only 20 s of IR + UV exposure at 1.8 K. The $R_1(0)$ feature is clearly more intense after only 20 s of IR + UV irradiation compared to the $R_1(0)$ feature after 41 min of UV photolysis (see Figure 1). This intensity difference in the $R_1(0)$ peak in trace (b) of Figures 1 and 3 clearly signals qualitatively new HCl photoproduction kinetics for the IR + UV irradiation scheme. It is also interesting to notice that the $(HCl)_2$ peaks that were evident in trace (b) of Figure 1 are not as prominent in Figure 3. The spectrum in trace (c) of Figure 3 is recorded after 164 min of IR + UV irradiation, and the HCl $R_1(0)$ absorption feature has nearly reached its maximum value.

To study the kinetics of HCl growth in the IR + UV photolysis experiment, again, the integrated absorbance of the HCl $R_1(0)$ transition is plotted as a function of IR + UV irradiation time. The same HCl integration limits used to analyze the UV data are used in the IR + UV experiment, and the results are plotted in Figure 4 as open circles. Analysis of the IR + UV data is complicated by two possible reaction mechanisms that can lead to HCl production. The first mechanism is consecutive reactions 2 and 4 where the nascent Cl* atom reacts directly with $H_2(v=1)$ to form HCl. The second mechanism consists of consecutive reactions 2 and 5 where the Cl atom becomes equilibrated in the p-H_2 matrix after photodissociation and then reacts with $H_2(v=1)$ via the IR-induced reaction studied previously, that is, reaction 5. To take advantage of all of the IR + UV kinetic data, the data are fit to the following expression appropriate for two sets of consecutive reactions with a common initial step[46]

$$y = \frac{a_4}{k_4 - k_2}[k_4(1 - e^{-k_2 t}) - k_2(1 - e^{-k_4 t})] + \frac{a_5}{k_5 - k_2}[k_5(1 - e^{-k_2 t}) - k_2(1 - e^{-k_5 t})] \quad (8)$$

The a_4 parameter denotes the maximum HCl integrated intensity at $t = \infty$ for HCl formed via reaction 4; similarly, a_5 denotes the maximum HCl integrated intensity for HCl produced via reaction 5, and the rate constants k_2, k_4, and k_5 represent rate constants for reactions 2, 4, and 5, respectively. The results of the fit of the IR + UV data to eq 8 are shown as a solid line in

TABLE 2: IR + UV Photolysis Fitted Constants

	a_4/cm^{-1}	a_5/cm^{-1}	k_2/min^{-1}	k_4/min^{-1}	k_5/min^{-1}
IR + UV	0.97(4)	5.32(4)	0.47(4)	20(12)	0.0213(3)

Figure 4 labeled total, and the fitted parameters are reported in Table 2. The k_5 rate constant extracted from the IR + UV data (0.0213(3) min^{-1}) is found to be slightly larger than the rate constant (0.0134(2) min^{-1}) measured for the IR-induced reaction reported in Table 1. The increase likely reflects the larger FTIR aperture diameter used in the IR + UV experiments (12.5 versus 4.0 mm). The k_2 rate constant ($k_2 = \sigma_{355} I_{355} \Phi$) is consistent with the known 355 nm cross section[42] and UV laser flux used in these experiments with a quantum yield (Φ) for Cl atom production of $\Phi = 0.35$. This value of the quantum yield for Cl-atom 355 nm photoproduction agrees with the quantum yield ($\Phi = 0.30$) measured in separate UV-only experiments determined by monitoring the extent of Cl_2 photolysis using the Cl spin−orbit transition.[43] The slight increase in the Cl-atom quantum yield under IR + UV conditions may be real and suggests that infrared absorptions of the p-H_2 solid may increase the probability that the Cl_2 molecule photodissociates after absorption of an UV photon. Finally, the k_4 rate constant extracted from the fit of the IR + UV data has the largest uncertainty but is significantly larger than the k_5 rate constant. This explains the shape of the data at early IR + UV photolysis times because if HCl was produced via reactions 2 and 5 only, the growth in the HCl integrated absorbance could not be reproduced at early time. The fact that three rate constants can be extracted from the IR + UV kinetic data relies on the rate constants being significantly different in magnitude. Thus, since the rate constant for reaction 5 is by far the slowest, at early IR + UV photolysis times, the HCl production is dominated by consecutive reactions 2 and 4.

Similar to the kinetic analysis of the UV data, the IR + UV HCl growth kinetics can be analyzed to estimate the reaction probability for reaction 4. The amount of HCl generated via the direct reaction of translationally hot Cl* with $H_2(v=1)$ can be determined from the fit to the HCl growth kinetics. Included in Figure 4 are plots of the two individual contributions to the total HCl production extracted from the fit to eq 8. The curve labeled IR + UV in Figure 4 plots the contribution to HCl production due to consecutive reactions 2 and 4, while the curve labeled IR plots the contribution due to consecutive reactions 2 and 5. For the direct reaction mechanism, since $k_4 > k_2$, the HCl growth curve labeled IR + UV increases very rapidly at early times. In contrast, for the delayed reaction mechanism labeled IR, since $k_5 < k_2$, the growth of HCl at early times is very slow since the Cl atom concentration needs to build up before reaction 5 can proceed at a significant rate.

The fraction of HCl molecules produced via consecutive reactions 2 and 4 can be determined from the fitted parameters in Table 2 and the following expression

$$P_R^{IR+UV} = \frac{a_4}{(a_4 + a_5)} \tag{9}$$

For the experimental data presented in Figure 4, the fraction of HCl molecules produced via IR + UV photolysis is $P_R^{IR+UV} = 0.154(8)$. Comparison of this reaction probability with the one determined for UV photolysis, $P_R^{UV} = 0.0056(1)$, shows an increase in the reaction probability by a factor greater than 25. This large increase reflects the qualitatively different microscopic dynamics of the photodissociation event for the two photolysis schemes, UV and IR + UV. Such large differences are only possible because (1) under these reaction conditions, the Cl + $H_2(v=1)$ reaction must have a significantly larger cross section than Cl + $H_2(v=0)$ and (2) the amount of $H_2(v=1)$ generated with broad-band IR irradiation of the sample is sufficient to make the rate of reaction 4 significant.

4. Discussion

(a) UV-Photoinitiated Cl + $H_2(v=0)$ → HCl + H Reaction in Solid p-H_2. The 355 nm photolysis of Cl_2 in a p-H_2 matrix at ~2 K produces almost exclusively (99.39%) isolated Cl atoms.[19−21] Even though the nascent Cl* atom is ejected with 4090 cm^{-1} of kinetic energy, it does not react with the matrix host, but rather, this excess translational energy is dissipated to the matrix through a number of nonreactive collisions, and the Cl atom becomes trapped below the barrier to reaction. In fact, our group has utilized in situ UV photolysis of dihalogen precursor molecules (Cl_2 and Br_2) to generate halogen-atom-doped solid p-H_2 to study IR-induced chemical reactions[20,43] and as a means to synthesize Br−HBr entrance channel complexes.[47] Insight into the lack of reactivity of the photo-ejected Cl* atom was provided by the simulations of Manz and co-workers that are presented in the accompanying paper.[9]

For a chemical reaction to proceed, the translational energy of the reacting partners and the center-of-mass (com) collision energy must be considered. If we examine the kinematics for a head-on collision between a fast-moving Cl atom and a single H_2 molecule essentially at rest (zero-point translational motion), the Manz group showed that the fraction of energy available for reaction (E_{rxn}) in the com frame is simply related to the masses of the two particles

$$\frac{E_{rxn}}{E_{trans}} = \frac{2m_H}{(m_{Cl} + 2m_H)} = 0.054 \tag{10}$$

Thus, the maximum energy E_{rxn} available for reaction between the nascent Cl* atom and a neighboring p-H_2 molecule under these photolysis conditions would only be about 220 cm^{-1}. Such a low collision energy is well below the threshold for the Cl + $H_2(v=0)$ reaction (~1500 cm^{-1}) and is also less than the endothermicity of the reaction.[14] However, the assumption that the Cl atom collides with a single p-H_2 molecule is not entirely correct since the target p-H_2 molecule is embedded in a quantum crystal. Thus, the maximum collision energy in a head-on collision within the solid should be slightly greater since the target p-H_2 molecule is in contact with nearest-neighbor p-H_2 molecules; regardless, given the weak intermolecular bonds between the p-H_2 molecules, it is hard to imagine that the collision energy could approach the 1500 cm^{-1} threshold value. Therefore, the UV photolysis measurements are consistent with the kinematics for photodissociation of the heavy Cl_2 molecule in a light p-H_2 matrix such that the com collision energy is below the threshold to reaction and photolysis results predominantly in isolated Cl atoms.

Given the discussion above, it is surprising that any HCl is generated during the in situ UV photolysis of Cl_2 in p-H_2. Indeed, the Manz group reports a reaction probability of $P_R^{UV} = 1.6 \times 10^{-5}$ and suggests that zero-point translational energy in the H_2 collision partner may be responsible for the nonzero reaction probability.[9] Specifically, the uncertainty in position of the H_2 collision partner due to translational zero-point motion within the quantum solid translates into uncertainty in the

momentum of the particle via the Heisenberg uncertainty relationship. As the uncertainty in the H_2 position is increased, the Manz group simulations show that the reaction threshold decreases due to the lesser uncertainty in the momentum of the H_2 molecule, where the high momentum components of the wave function have a greater reaction probability. These calculations suggest that the extent of translational zero-point motion can influence the threshold behavior of the UV-initiated $Cl + H_2(v=0)$ reaction in solid p-H_2.

The measured nonzero P_R^{UV} reaction probability presented here may also contain contributions of HCl production due to reactions other than consecutive reactions 2 and 3. Experiments conducted with higher initial Cl_2 concentrations (e.g., 120 ppm) show increased UV reaction probabilities. While further experiments need to be conducted, the initial results seem to suggest that at the higher Cl_2 concentrations, additional side reactions become significant during UV photolysis. For example, the probability of Cl-atom recombination is increased, and reforming Cl_2 releases approximately 20000 cm^{-1} of energy, which may trigger reactions of Cl with H_2 and/or further recombination and agglomeration. In addition, the effect of the UV laser flux needs be tested since the 355 nm photolysis beam can potentially induce stimulated Raman processes in the p-H_2 solid.[48,49] These Raman processes excite pure $H_2(v=1)$ vibrons, which can lead to HCl production via reactions 4 or 5. Accordingly, experiments at low initial Cl_2 concentrations and at low laser fluxes should produce the best measurement of the P_R^{UV} reaction probability. The average reaction probability $P_R^{UV} = 0.0061(30)$ presented here was determined from measurements on five distinct crystals with initial Cl_2 concentrations of less than 50 ppm and UV laser energies of 2 and 4 mJ. Therefore, this reaction probability is the best estimate based on the available data, and further experiments are underway to determine the lower limit of this quantity.

This approach of using in situ UV photolysis of Cl_2 in solid p-H_2 offers a new way to study the $Cl(^2P_{3/2}) + H_2(v=0,J=0)$ reaction in a condensed-phase environment. The crystal structure of the quantum matrix allows for a very homogeneous condensed-phase system such that the dynamics should be simplified since all reactions start from a single well-defined initial state. It allows for the reaction to be probed at very low collision energies, given the discussion above, where a translationally hot heavy species is created in the light p-H_2 matrix. Upon the basis of the gas-phase measurements, the Cl-atom reagent is produced almost exclusively (99.4%) in the ground spin−orbit ($^2P_{3/2}$) state.[22−24] Photodissociation of a molecular precursor isolated in solid p-H_2 using nanosecond lasers produces a very narrow translational energy distribution of the reagent Cl* atoms. In addition, the quantum labels on all of the p-H_2 molecules are equally well-defined. The matrix host is enriched to 99.99% p-H_2, ensuring that the H_2 molecules are in $J = 0$ rotational states. At liquid helium temperatures, the thermal population of the $H_2(v=1)$ excited vibrational state (4153 cm^{-1}) is vanishingly small. Optical pumping of solid p-H_2 by blackbody radiation from the room is also not a significant source of $H_2(v=1)$ since the region where solid p-H_2 absorbs (4000−5000 cm^{-1}) is on the high-energy side of the 300 K blackbody curve where the intensity falls off sharply. In the region where solid p-H_2 absorbs, the radiant energy density is at least 10000 times less than that at the peak of the blackbody curve near 1000 cm^{-1}. The sample is also shielded from blackbody radiation with only three small holes cut in the radiation shield to allow optical access.

The photodissociation of a small molecule like Cl_2 in a quantum matrix of p-H_2 molecules is a condensed-phase photochemical problem that we still know very little about and where theory is needed to provide more insight. For example, a basic question such as how far the Cl atom migrates, on average, after photodissociation of Cl_2 and before it comes into equilibrium in solid p-H_2 is not known. Classical molecular dynamics simulations of F_2 photodissociation in Ar crystals revealed a wealth of dynamical information.[4] Given that the de Broglie wavelength associated with each p-H_2 molecule in a quantum matrix is significant and that zero-point motion should be accounted for in solid p-H_2, it is not clear if similar classical molecular dynamics simulations would be able to reproduce the true dynamics. Another basic question is how the translational energy of the Cl* atom is dissipated to the matrix. Are phonons, rotons, and/or vibrons excited in the process? Much is known about the photodissociation of small molecules in Rg matrixes, and thus, some of the experimental and theoretical techniques may be transferred to study photodissociation in a quantum matrix of p-H_2.

(b) IR + UV-Photoinitiated $Cl + H_2(v=1) \rightarrow HCl + H$ Reaction in Solid p-H_2. In contrast to the UV photodissociation results, simultaneous IR + UV irradiation of Cl_2 in solid p-H_2 under the conditions studied resulted in greater than 15% of the photoejected Cl* atoms reacting with the p-H_2 host. We attribute this increased reaction probability to the significantly enhanced reaction cross section at low collision energies for the $Cl + H_2(v=1)$ reaction. On the basis of the quasiclassical trajectory studies of Broida and co-workers,[17] the reaction threshold drops from 1400 cm^{-1} for $Cl + H_2(v=0)$ to 350 cm^{-1} for $Cl + H_2(v=1)$. Furthermore, these calculations[17] indicate that near threshold, the reaction cross section for reaction with $H_2(v=1)$ is 0.48 $Å^2$, whereas it is only 0.025 $Å^2$ for $H_2(v=0)$. Unfortunately, Broida and co-workers only reported the $Cl + H_2(v=0)$ cross section near threshold for $J = 1$ *ortho*-hydrogen (o-H_2) and not $J = 0$ p-H_2, but on the basis of the reaction cross sections, these trajectory calculations predict an enhancement by a factor of 20. The calculated enhancement of the reaction rate with vibrational excitation of the H_2 reagent is also expected from Polanyi's rules for late barrier reactions.[18] Polanyi was the first to point out that for thermoneutral three-atom exchange reactions with appreciable late reaction barriers, vibrational excitation of the reagent is much more effective at surmounting the barrier than translational energy.

The quantum dynamic simulations of the Manz group presented in the accompanying paper[9] also support this interpretation that the increased reaction probability under IR + UV photolysis conditions is due to consecutive reactions 2 and 4. The wavepacket simulations show that $H_2(v=1)$ vibrational preexcitation dramatically increases the reaction probability from $P_R^{UV} = 1.6 \times 10^{-5}$ to $P_R^{IR+UV} = 0.6$. Part of this increase in the reaction probability is purely an energetic effect; the total energy (vibration + translation) available for the $Cl + H_2(v=1)$ reaction under IR + UV photolysis conditions is much larger than the total energy of the $Cl + H_2(v=0)$ reaction initiated by UV photolysis. However, the wavepacket simulations also showed a significant dynamical propensity for putting the energy into vibrational excitation of the H_2 reagent. Manz also conducted simulations at the same total energy as the IR + UV simulation, but where all of the energy was in the form of translational energy of the Cl atom, and observed a reaction probability $P_R = 0.36$, which is significantly lower. The simulated wavepacket dynamics led the authors to present an "interpolated Polyani rule" for the $Cl + H_2$ reaction which states that equal amounts

of vibrational and translational energy should be best suited to overcome the reaction barrier.[9]

The calculated IR + UV reaction probability cannot be compared directly with the measured value because the quantum simulations assume that every nascent Cl* atom is directed toward and collides with a single neighboring vibrationally excited $H_2(v=1)$ molecule. In contrast, this assumption is difficult to achieve experimentally since the IR excitation step only excites a small fraction of the H_2 molecules. As a consequence, the calculated IR + UV reaction probability truly represents an upper limit to the experimental value. In fact, the measured value $P_R^{IR+UV} = 0.154$ is 25% of the limiting theoretical value, which suggests that in one-forth of the IR + UV photolysis reactions, the nascent Cl collides with a $H_2(v=1)$ reaction partner. Given that it is highly unlikely that one-forth of all of the H_2 molecules are vibrationally excited, the high reaction probability measured under IR + UV photolysis conditions suggests that some additional and, as yet, unknown enhancement in the reaction probability is occurring in the p-H_2 solid.

An important finding of this work is that the dynamics of the Cl + H_2 reaction seem to be preserved when the reaction takes place in a p-H_2 solid presumably because the quantum states of the reactants are well-defined. Through comparison with the wavepacket simulations presented in the accompanying paper, the enhanced reaction probability measured for the IR + UV photolysis scheme results partly from the dynamical preference of the Cl + H_2 reaction for energy in the form of vibrational excitation of the H_2 reagent. The measured dynamical preference should also exist in the gas-phase reaction, and thus, conducting the reaction in a p-H_2 solid does little to perturb the basic reaction dynamics. This, therefore, opens the possibility to study the vibrational enhancement of the rates of reactions involving atoms and molecules with H_2 in solid p-H_2 matrixes especially when the analogous gas-phase reaction studies prove difficult.

What we feel is surprising is that the weak broad-band IR source can generate sufficient $H_2(v=1)$ excited states so that when the Cl_2 molecule dissociates, the nascent Cl* atom has a finite probability of colliding with a $H_2(v=1)$ molecule and reacting before it returns to equilibrium in the p-H_2 matrix. The translationally hot Cl* atoms are generated 10 times a second with nanosecond laser pulses. As previously mentioned, it is difficult to estimate how long it takes for the photoejected Cl* atom to dissipate its translational energy and come to rest in the matrix, and this is an area where theoretical studies would be very helpful. We show from fits to the HCl growth curve during IR + UV irradiation that more than 15% of the HCl produced is due to reactions of translationally hot Cl* atoms with $H_2(v=1)$ because we do not observe significant HCl generation during UV-only photolysis and the measured IR+UV HCl photoproduction kinetics cannot be reproduced by consecutive reactions 2 and 5 alone. The individual rate constants for reactions 2 and 5 are well characterized under these experimental conditions, and since the rate constant for reaction 5 is much less than that for reaction 2 ($k_5 \ll k_2$), the qualitative shape of the HCl growth curve cannot be reproduced without inclusion of another reaction mechanism that produces HCl.

These are preliminary measurements, and there are a variety of issues that need further study, specifically the roles of (1) phonon excitation, (2) $J = 1$ o-H_2 impurities, and (3) Cl_2- or Cl-induced $Q_1(0)$ transitions in the observed reaction kinetics. First, the p-H_2 solid absorbs IR radiation via the $Q_R(0)$, $Q_1(0)$ + $S_0(0)$, and $S_R(0)$ transitions such that there is a broad continuous absorption from 4200 to 4800 cm^{-1} due to the solid p-H_2 matrix. This 600 cm^{-1} broad absorption profile is well matched to the peak in the intensity of the near-IR light emitted by the broad-band tungsten source, and we speculate that it is the dominant absorption mechanism that generates the vibrons necessary to induce chemistry. However, both of the broad $Q_R(0)$ and $S_R(0)$ phonon sideband absorptions result not only in delocalized vibron excitation but also in phonon excitation. It is not clear if phonon excitation plays a role in the enhanced IR + UV photochemistry. Second, in the studies presented here, the concentration of $J = 1$ o-H_2 impurities was minimal (<300 ppm), and accordingly, these species are not expected to play a role in the current reaction studies. However, at elevated o-H_2 concentrations (e.g., 10%), the o-H_2-induced $Q_1(0)$ transition could provide an additional absorption mechanism to generate $H_2(v=1)$ vibrons and thus possibly increase the IR + UV reaction probability. Competitively, at elevated o-H_2 concentrations, the mean free path of the $H_2(v=1)$ vibron decreases, which would decrease the IR + UV reaction probability. Clearly, the effect of elevated o-H_2 concentrations on the IR + UV reaction probability requires additional study. Finally, both the Cl_2 and Cl atom-induced $Q_1(0)$ absorptions lead to vibron excitation in p-H_2 molecules directly in contact with the impurity. Thus, these transitions could selectively excite the reaction partners and therefore might be responsible for the high reaction probabilities measured under IR + UV photolysis conditions that nearly reach the maximum theoretical limit. We speculate that this is not the case since the Cl_2- and Cl-induced $Q_1(0)$ transitions are relatively sharp, and thus, the amount of light absorbed via these transitions by a broad-band source in comparison with the 600 cm^{-1} broad solid p-H_2 absorptions is negligible. However, we cannot rule out the contributions of these absorptions because we cannot selectively excite only the Cl_2-induced $Q_1(0)$ transitions.

Only through collaboration with theory will we be able to understand the vibrationally enhanced low-temperature chemistry that is occurring in solid p-H_2. To better quantify the relative rates for reactions 3 and 4 under these conditions, we need to know how many collisions it takes on average for the photoejected Cl* atom to dissipate its energy. The number of collisions that occur before equilibration will help determine how the reaction probability increases with vibrational excitation since if Cl* atom equilibration occurs very rapidly, the reaction cross section would have to be much larger to measure an effect. Further, we need to estimate the effective concentration of $H_2(v=1)$ vibrons that are generated under these conditions and to begin to investigate the essentially unexplored reaction dynamics of the Cl* atom reacting with the $H_2(v=1)$ delocalized vibrons in solid p-H_2. Since the $v=1$ vibron is delocalized within the solid, the vibrational energy is not localized on a single p-H_2 molecule but rather is delocalized over many p-H_2 molecules via a tight-binding-like Hamiltonian.[8,50] The physical picture that emerges is that at any instance in time, the vibrational excitation is distributed over a collection of p-H_2 molecules (say 13, a central molecule and its 12 nearest neighbors) with amplitudes and phases determined by the vibron wave function. This delocalization of the vibrational energy over many p-H_2 molecules, therefore, likely results in a larger "reactive cross section" for collision of the Cl* atom with the $v = 1$ vibron than it would be if the vibrational excitation was localized on a single p-H_2 molecule in the crystal.

5. Conclusions

The photodissociation of Cl_2 in solid p-H_2 matrixes at 1.8 K is studied using two different photolysis schemes, namely, UV

and IR + UV, where the UV radiation is the 355 nm output of a nanosecond Nd:YAG laser and the IR radiation is cw broadband near-IR light produced by a water-cooled tungsten source of a FTIR spectrometer. The extent of the photochemistry is followed by measuring the integrated absorbance of the $R_1(0)$ rovibrational transition of the HCl reaction product. The IR + UV photolysis experiments show evidence in the measured HCl growth curves that the reaction $Cl^* + H_2(v=1,J=0) \rightarrow HCl + H$ is playing a significant (15%) role in the photochemistry. In contrast, UV photolysis produces nearly exclusively Cl atoms, which indicates that under these conditions, the reaction $Cl^* + H_2(v=0,J=0) \rightarrow HCl + H$ is not readily occurring. Accordingly, these results are consistent with significant enhancement in the rate of the $Cl + H_2 \rightarrow HCl + H$ reaction with vibrational excitation of the H_2 reagent. The IR + UV results are particularly interesting since they indicate that the translationally hot Cl* atom generated via in situ UV photolysis has a finite probability of reacting with a delocalized $v = 1$ vibron in the solid before it dissipates the excess photolysis energy and returns to thermal equilibrium within the p-H_2 solid. From the excess energy imparted to the Cl* atom and an analysis of the kinematics of $Cl + H_2$ collisions, these rather unique condensed-phase reaction dynamics are found to be occurring at rather low center-of-mass collision energies (220 cm^{-1}). The interpretation of these photochemical results is supported by the wavepacket simulations presented in the accompanying paper by Manz and co-workers,[9] namely, that the dramatically enhanced HCl reaction probability measured under IR +UV photolysis conditions results from contributions of the $Cl + H_2(v=1)$ reaction. These results illustrate how IR + UV photochemical studies can be used with chemically doped solid p-H_2 crystals to study H_2 vibrational enhancement of simple chemical reactions in a condensed-phase environment.

Acknowledgment. The authors would like to thank the Schwentner group for their gracious hospitality during the sabbatical stay in their research group that led to the collaboration with the Manz group and ultimately the present work. This research was sponsored by the Chemistry Division of the U.S. National Science Foundation (CHE 03-16268) and by the Deutsch Forschungsgemeinschaft (Sfb 450).

References and Notes

(1) Perutz, R. N. *Chem. Rev.* **1985**, *85*, 97.
(2) Apkarian, V. A.; Schwentner, N. *Chem. Rev.* **1999**, *99*, 1481.
(3) Alimi, R.; Brokman, A.; Gerber, R. B. *J. Chem. Phys.* **1989**, *91*, 1611.
(4) Alimi, R.; Gerber, R. B.; Apkarian, V. A. *J. Chem. Phys.* **1990**, *92*, 3551.
(5) Bargheer, M.; Cohen, A.; Gerber, R. B.; Gühr, M.; Korolkov, M. V.; Manz, J.; Niv, M. Y.; Schröder, M.; Schwentner, N. *J. Phys. Chem. A* **2007**, *111*, 9573.
(6) Cohen, A.; Gerber, R. B. *Chem. Phys. Lett.* **2008**, *453*, 173.
(7) Nosanow, L. H. *Phys. Rev.* **1966**, *146*, 120.
(8) Van Kranendonk, J. *Solid Hydrogen - Theory of the Properties of Solid H_2, HD, and D_2*; Plenum Press: New York, 1983.
(9) Korolkov, M. V.; Manz, J.; Schild, A. *J. Phys. Chem. A* **2009**, *113*, 7630.
(10) Allison, T. C.; Mielke, S. L.; Schwenke, D. W.; Lynch, G. C.; Gordon, M. S.; Truhlar, D. G. *Gas-Phase Reaction Systems: Experiments and Models 100 Years after Max Bodenstein*; Springer-Verlag: Berlin, Germany, 1996; p 111.
(11) Alagia, M.; Balucani, N.; Cartechini, L.; Casavecchia, P.; Kleef, E. H. v.; Volpi, G. G.; Aoiz, F. J.; Bañares, L.; Schwenke, D. W.; Allison, T. C.; Mielke, S. L.; Truhlar, D. G. *Science* **1996**, *273*, 1519.
(12) Alagia, M.; Balucani, N.; Cartechini, L.; Casavecchia, P.; Volpi, G. G.; Aoiz, F. J.; Banares, L.; Allison, T. C.; Mielke, S. L.; Truhlar, D. G. *Phys. Chem. Chem. Phys.* **2000**, *2*, 599.
(13) Capecchi, G.; Werner, H.-J. *Phys. Chem. Chem. Phys.* **2004**, *6*, 4975.
(14) Lee, S.-H.; Lai, L.-H.; Liu, K.; Chang, H. *J. Chem. Phys.* **1999**, *110*, 8229.
(15) Lee, S.-H.; Liu, K. *J. Chem. Phys.* **1999**, *111*, 6253.
(16) Wang, X.; Dong, W.; Xiao, C.; Che, L.; Ren, Z.; Dai, D.; Wang, X.; Casavecchia, P.; Yang, X.; Jiang, B.; Xie, D.; Sun, Z.; Lee, S.-Y.; Zhang, D. H.; Werner, H.-J.; Alexander, M. H. *Science* **2008**, *322*, 573.
(17) Persky, A.; Rubin, R.; Broida, M. *J. Chem. Phys.* **1983**, *79*, 3279.
(18) Polanyi, J. C. *Acc. Chem. Res.* **1972**, *5*, 161.
(19) Yoshioka, K.; Raston, P. L.; Anderson, D. T. *Int. Rev. Phys. Chem.* **2006**, *25*, 469.
(20) Raston, P. L.; Anderson, D. T. *Phys. Chem. Chem. Phys.* **2006**, *8*, 3124.
(21) Raston, P. L.; Anderson, D. T. *J. Chem. Phys.* **2007**, *126*, 021106.
(22) Matsumi, Y.; Tonokura, K.; Kawasaki, M. *J. Chem. Phys.* **1992**, *97*, 1065.
(23) Samartzis, P. C.; Bakker, B. L. G.; Rakitzis, T. P.; Parker, D. H.; Kitsopoulos, T. N. *J. Chem. Phys.* **1999**, *110*, 5201.
(24) Kokh, D. B.; Alekseyev, A. B.; Buenker, R. J. *J. Chem. Phys.* **2004**, *120*, 11549.
(25) Christophorou, L. G.; Olthoff, J. K. *J. Phys. Chem. Ref. Data* **1999**, *28*, 131.
(26) Marushkevich, K.; Khriachtchev, L.; Rasanen, M. *Phys. Chem. Chem. Phys.* **2007**, *9*, 5748.
(27) Fajardo, M. E.; Tam, S. *J. Chem. Phys.* **2001**, *115*, 6807.
(28) Fushitani, M.; Momose, T.; Shida, T. *Chem. Phys. Lett.* **2002**, *356*, 375.
(29) Momose, T.; Fushitani, M.; Hoshina, H. *Int. Rev. Phys. Chem.* **2005**, *24*, 533.
(30) Momose, T.; Hoshina, H.; Sogoshi, N.; Katsuki, H.; Wakabayashi, T.; Shida, T. *J. Chem. Phys.* **1998**, *108*, 7334.
(31) Momose, T.; Masaki, M.; Uchida, M.; Shimizu, T.; Yoshizawa, I. *J. Chem. Phys.* **1995**, *103*, 1400.
(32) Momose, T.; Uchida, M.; Sogoshi, N.; Miki, M.; Masuda, S.; Shida, T. *Chem. Phys. Lett.* **1995**, *246*, 583.
(33) Fushitani, M.; Shida, T.; Momose, T.; Rsnen, M. *J. Phys. Chem. A* **2000**, *104*, 3635.
(34) Raston, P. L.; Anderson, D. T. *Low Temp. Phys.* **2007**, *33*, 487.
(35) Hinde, R. J. *J. Chem. Phys.* **2003**, *119*, 6.
(36) Fajardo, M. E.; Tam, S. *J. Chem. Phys.* **1998**, *108*, 4237.
(37) Tam, S.; Fajardo, M. E. *Rev. Sci. Instrum.* **1999**, *70*, 1926.
(38) Yoshioka, K.; Anderson, D. T. *J. Mol. Struct.* **2006**, *786*, 123.
(39) Tam, S.; Fajardo, M. E.; Katsuki, H.; Hoshina, H.; Wakabayashi, T.; Momose, T. *J. Chem. Phys.* **1999**, *111*, 4191.
(40) Anderson, D. T.; Hinde, R. J.; Tam, S.; Fajardo, M. E. *J. Chem. Phys.* **2002**, *116*, 594.
(41) Skvortsov, D.; Choi, M. Y.; Vilesov, A. F. *J. Phys. Chem. A* **2007**, *111*, 12711.
(42) Hubinger, S.; Nee, J. B. *J. Photochem. Photobiol. A: Chem.* **1995**, *86*, 1.
(43) Raston, P. L.; Anderson, D. T. Manuscript in preparation.
(44) Souers, P. C. *Hydrogen Properties for Fusion Energy*; University of California Press: Berkeley, CA, 1986.
(45) Kettwich, S. C.; Paulson, L. O.; Raston, P. L.; Anderson, D. T. *J. Phys. Chem. A* **2008**, *112*, 11153.
(46) Laidler, K. *Chemical Kinetics*, 3rd ed.; Harper & Row, Publishers, Inc.: New York, 1987.
(47) Kettwich, S.; Pinelo, L.; Anderson, D. T. *Phys. Chem. Chem. Phys.* **2008**, *10*, 5564.
(48) McCall, B. J.; Huneycutt, A. J.; Saykally, R. J.; Lindsay, C. M.; Oka, T.; Fushitani, M.; Miyamoto, Y.; Momose, T. *Appl. Phys. Lett.* **2003**, *82*, 1350.
(49) Kuyanov, K. E.; Momose, T.; Vilesov, A. F. *Appl. Opt.* **2004**, *43*, 6023.
(50) Feldman, J. L.; Eggert, J. H.; Kinder, J. D.; Hemley, R. J.; Mao, H.-k.; Schoemaker, D. *Phys. Rev. Lett.* **1995**, *74*, 1379.

JP811206A